

DTIC

ELECTE

NOV 14 1989

THE RESPONSE OF HELICOPTER ROTORS TO VIBRATORY AIRLOAD

William G. Bousman

U.S. Army Aeroflightdynamics Directorate (AVSCOM)
Ames Research Center, Moffett Field, California 94035

ABSTRACT

Structural response data from flight or wind tunnel tests of eight full-scale rotors have been examined and compared for high-speed flight conditions and in the absence of blade stall or maneuvers. Both similarities and differences in the behavior of the rotors were observed, and these findings are useful in determining appropriate tests for the development of theoretical methods. Limited use is made of airload measurements and theoretical calculation in examining these data. Major similarities observed in the rotor behavior include: (1) 3/rev vibratory flap bending moments are remarkably similar among all the rotors at high speed; (2) the root oscillatory chord bending induced by lag dampers is similar for three of the articulated rotors despite differences in the damper type; and (3) the torsion moment and pitch-link loads show the same positive-negative loading over the advancing side of the disk caused by the unsteady pitching moments at the blade tip. Differences that were observed include: (1) the vibratory chord bending-moment behavior appears to be dependent on rotor stiffness in part, but differences seen are not easily explained; (2) the CH-53A root oscillatory chord bending-moment data do not show the damper-induced loads that are seen on the other articulated rotors with hydraulic lag dampers; and (3) the AH-1G torsion response is very different from that of the articulated rotors.

INTRODUCTION

The prediction of rotor vibratory airloads and structural loads remains a difficult and intractable problem. The development of improved theoretical methods requires careful comparison of theory and experiment, and demonstration that the theory does in fact correctly represent the physics of the problem. Within this context, the examination and comparison of measurements obtained for a wide range of full-scale rotors is valuable in that behaviors that are independent of rotor type as well as behaviors that depend upon the rotor configuration can be identified. Those behaviors that are common to many different rotors provide a first test of theoretical methods. To successfully pass this first test, a theory must properly model the physics of helicopter rotors in forward flight. It is not sufficient, for example, to predict the magnitude of a loading component and miss the phase. In this sense, the predictions of a theoretical model must be at least as good as the estimates obtained from scaling previous flight test data. Once a theoretical model has shown that it

can pass the first test with some consistency, it must demonstrate that it can predict, as well, those behaviors that differ among rotor configurations. This is the second test. The objective of this paper is to seek appropriate tests for theoretical-methods development through comparison of full-scale rotor measurements.

Hooper, in Ref. 1, has examined the vibratory airloads obtained from tests of six full-scale rotors either in flight or in the wind tunnel. In each of these tests, pressure transducers were installed at multiple radial stations and the individual pressures were integrated to provide the normal force. The vibratory airload behavior has been visualized by means of computer graphics programs. This work has demonstrated that the vibratory airloads are remarkably consistent in the transition regime regardless of the number of blades, the rotor size, or the trim. At higher speeds many similarities are seen between the different rotors, but the blade airloading is more variable.

The present paper complements Hooper's work in that the problem of vibratory loading is examined largely from the perspective of the rotor structural response. This examination is valuable in its own right because the different perspective that is obtained assists in the understanding of a complex problem. In addition, by examining the rotor response it is possible to use data from tests in which only structural measurements have been obtained. This paper begins with a brief discussion of the scope of the paper and the data that were used. The problem of rotor response is then treated by discussing the blade flap, chord, and torsion responses separately. The rotor blade motions are, of course, coupled, but the separation used here is suitable for a qualitative examination. Important similarities between the rotors will be discussed as well as some fundamental differences. Conclusions from the comparisons will be made.

EXPERIMENTAL DATA

The comparisons shown are based on data obtained from eight flight-test or wind tunnel experiments on full-scale rotors.²⁻⁷ These are, for the most part, the only data that are accessible on magnetic storage media or tabulated in archive reports. Table 1 summarizes the eight sets of data and includes a description of the major instrumentation. The S-76 wind tunnel test reported in Ref. 5 included four interchangeable tips, but only the data from the swept/tapered (production) tip are shown here. Results of testing of the SA 330 Puma were reported in Refs. 8 and 9. The data used here are from the tests of an unusual mixed-bladed rotor configuration which had an instrumented swept tip installed on one blade and an instrumented rectangular tip installed on the opposite blade. The blades at 90° and 270° were the standard Puma blades. Data from a second test of the SA 349/2¹⁰ have also been examined, but are not shown in this paper as they are essentially identical to the measurements obtained

Paper presented at the American Helicopter Society National Specialists' Meeting on Rotorcraft Dynamics, Arlington, Texas, November 13-14, 1989.

Table 1. Full-Scale Rotor Data

AIRCRAFT	CONFIG.	TEST	INSTRUMENTATION ^a	REFERENCE
CH-34	Articulated, 4 blades	Flight	Differential pressure (7) Flap bending moment (6) Chord bending moment (3) Torsion moment (2) Pitch-link load	Scheiman, 1964
CH-34	Articulated, 4 blades	Wind tunnel	Differential pressure (9) Flap bending moment (4) Chord bending moment (4) Torsion moment (3)	Rabbott <i>et al.</i> , 1966
CH-53A	Articulated, 6 blades	Flight	Abs./diff. pressure (5) Flap bending moment (7) Chord bending moment (7) Torsion moment (2) Pitch-link load	Beno, 1970
S-76	Articulated, 4 blades	Wind tunnel	Flap bending moment (4) Chord bending moment (3) Pitch-link load	Johnson, 1980
AH-1G	Teetering, 2 blades	Flight	Absolute pressure (8) Flap bending moment (9) Chord bending moment (9) Torsion moment (5) Pitch-link load	Cross and Watts, 1988
SA-330 Puma	Articulated, 4 blades	Flight	Absolute pressure (3) Pitch-link load	
SA-349/2	Articulated, 3 blades	Flight	Absolute pressure (3) Flap bending moment (5) Chord bending moment (7) Torsion moment (4) Pitch-link load	Heffernan and Gaubert, 1986
UH-60A	Articulated, 4 blades	Flight	Flap bending moment (4) Chord bending moment (3) Pitch-link load	

^aThe number of the radial station with instrumentation is shown in parentheses.

in the first test. Data obtained during the UH-60A testing in 1987 are accessible through the TRENDS data base at Ames Research Center.

Flight and wind tunnel cases for trimmed, level flight were selected from the experimental data bases. The lift coefficients and advance ratios for the data used in this paper are shown in Fig. 1 compared to the rotor lift boundary obtained in Ref. 11 with a model-scale rotor. The lift coefficient values range from 0.06 to 0.08 and the maximum advance ratios are generally in the range of 0.35 to 0.40. In the case of the S-76, only data for the 0.38 advance ratio case were used. The rotor lift boundary that was obtained by McHugh¹¹ represents an aerodynamic limit rather than a structural limit because the model tested was sufficiently strong that the rotor collective pitch could be increased until the rotor thrust no longer increased. The rotor data that are examined in this paper were obtained at lift coefficients well below McHugh's rotor lift boundary, and therefore little or no stall is expected on the outer portion of the blade at any azimuth. For the experimental cases where aerodynamic loads data are avail-

able, this conclusion is confirmed by the absence of stall behavior in the pressure-transducer time histories.

Data are available for most of the rotors examined here over a full range of advance ratios. Hooper has clearly shown that all rotors respond strongly to the loading induced by the tip vortex of the previous blade in the low-speed or transition regime where the vortex passes very close to the blade. Although this area of the flight envelope remains highly interesting, the primary purpose of this paper is to examine the blade loading at the high-speed end of the aircraft envelope. Normal-force data measured at 95 ft on the rectangular tip of the SA 330 Puma⁸ are shown as a function of azimuth and advance ratio in Fig. 2, which illustrates how the character of the loading changes as airspeed is increased. The normal force is in the nondimensional form

$$M^2 C'_L = \frac{2L}{a^2 \rho}$$

where L is the lift, a is the speed of sound, and ρ is the density.

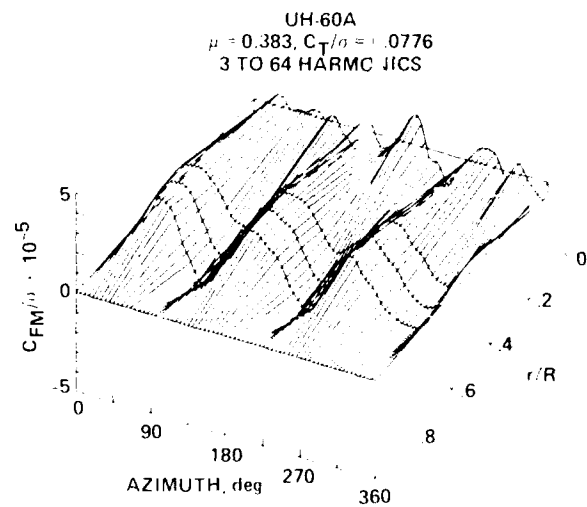
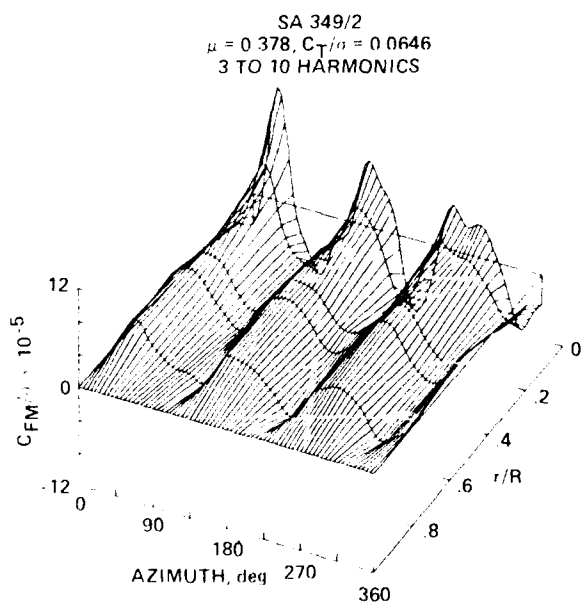
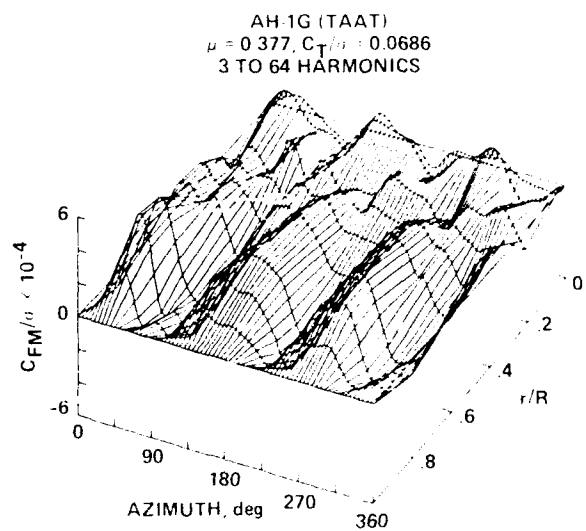
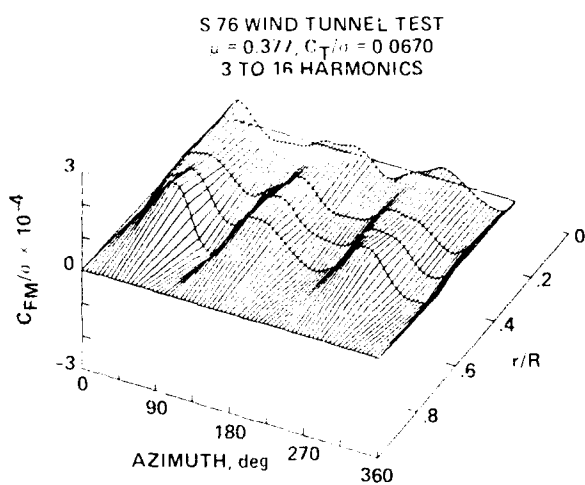
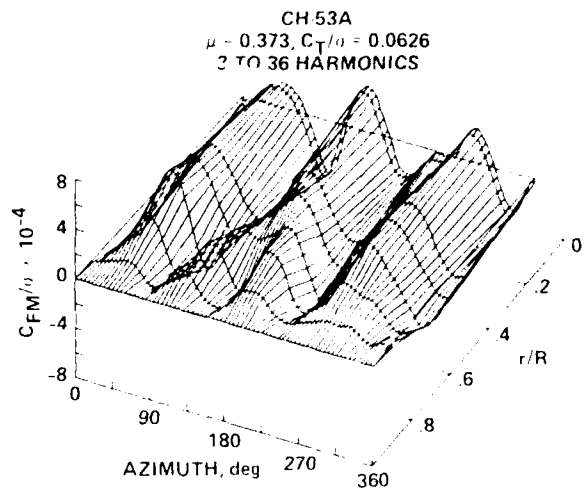
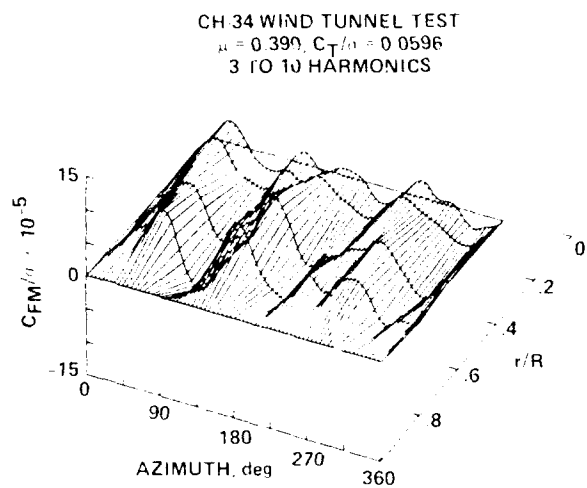


Fig. 4. Vibratory flap bending moments for six rotors at high speed as a function of radial station and azimuth.

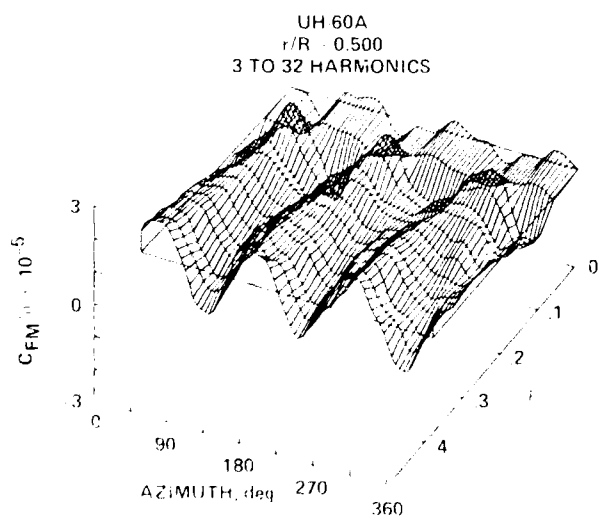
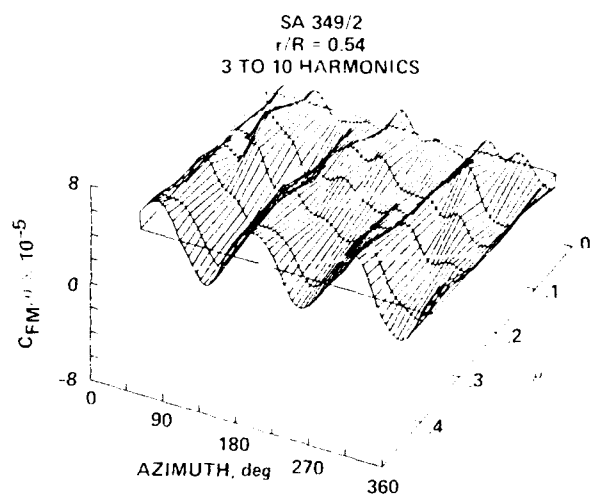
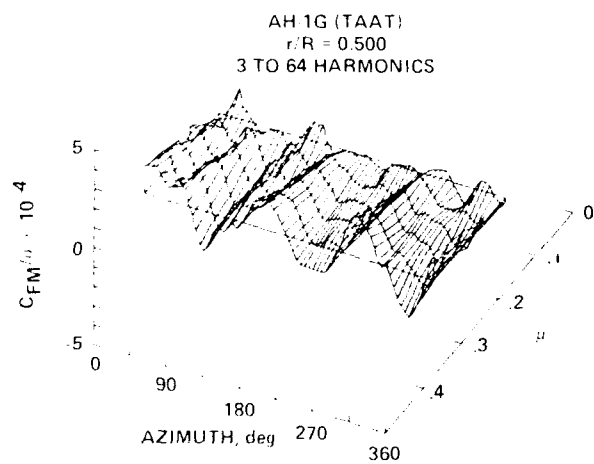
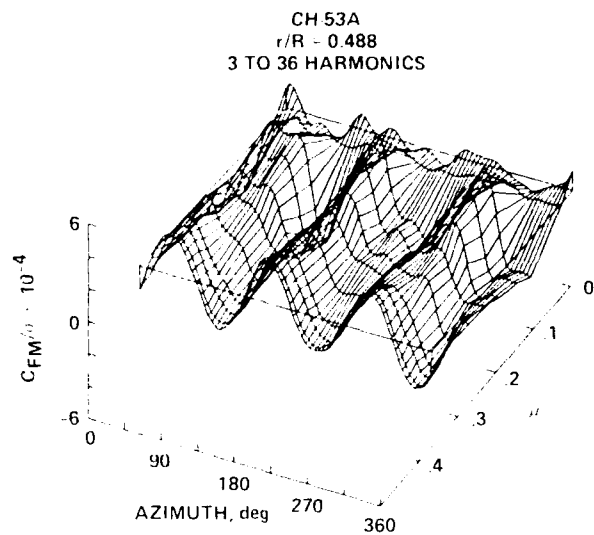
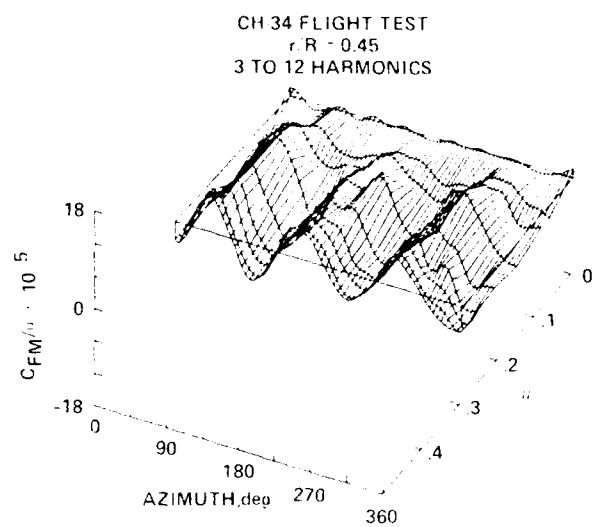


Fig. 5. Midspan rib-stress flap bending moments for five rotors as a function of advance ratio and azimuth.

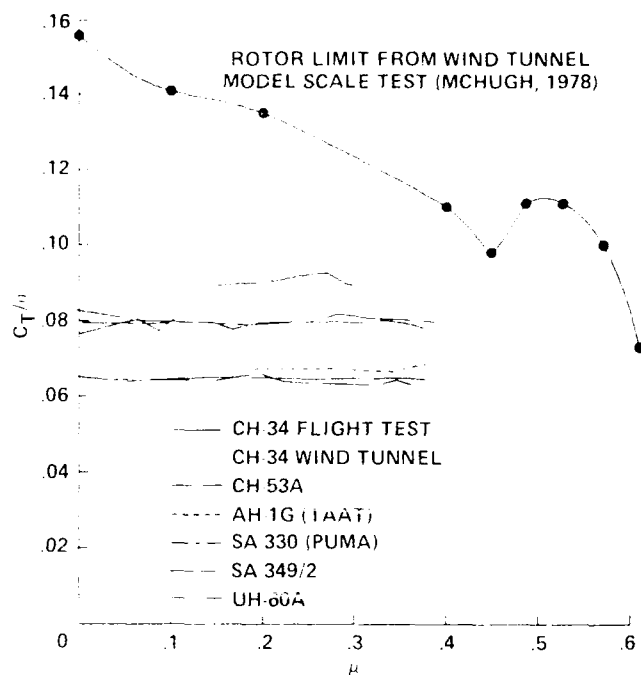


Fig. 1. Rotor lift coefficient and advance ratio of experimental data.

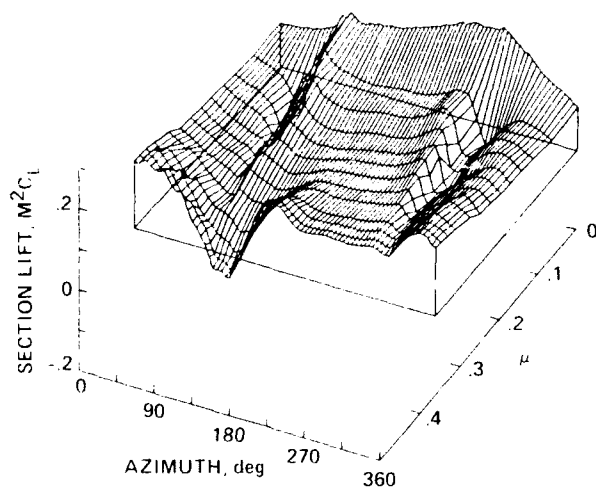


Fig. 2. Nondimensional normal force measured on SA 330 Puma as a function of azimuth and advance ratio; $r/R = 0.95$.

The Puma data shown in Fig. 2 were obtained on a mixed-bladed rotor configuration and are therefore not strictly representative of conventional rotors. However, the high resolution of the data in azimuth and advance ratio clearly exhibits the major features of the blade airloads as advance ratio is increased. At the lower advance ratios, the loading that is induced by the vortex of the previous blade is quite evident on both the advancing and the retreating sides of the disk. As expected, this loading is a sharp down-up pulse on the advancing side as the vortex moves radially inward, and is an up-down pulse on the retreat-

ing side as the vortex moves back out to the blade tip. Although the effect of the tip vortex on the retreating side is still detectable at the highest advance ratios, the vortex loading on the advancing side is no longer observed for $\mu \geq 0.3$. At the same time, the lift at the blade tip is decreasing on the advancing side of the disk so as to maintain roll-moment balance of the rotor. The primary purpose of this paper, then, is to examine the response of rotors in these high-speed conditions without the complicating effects of blade stall and maneuvers.

Two of the sets of rotor data examined by Hooper, the XH-51A compound¹² and the NH-3A compound,¹³ are interesting in their own right, but are not included in the present comparisons because of the confounding effects of wing lift and auxiliary propulsion.

FLAP BENDING-MOMENT RESPONSE

The flap mode frequencies of the rotors examined here are shown in a simplified form in Fig. 3. The frequencies are shown in terms of their endpoint values calculated at $0.4\Omega_0$ and $1.2\Omega_0$, where Ω_0 is the nominal rotor speed. This approach is an approximate method of indicating the uncoupled blade frequencies. Values for the CH-34, the SA 349/2, and the UH-60A have been calculated using CAMRAD. The frequencies for the CH-53A,⁴ the S-76,¹⁴ and the AH-1G¹⁵ are from calculations made by the manufacturer.

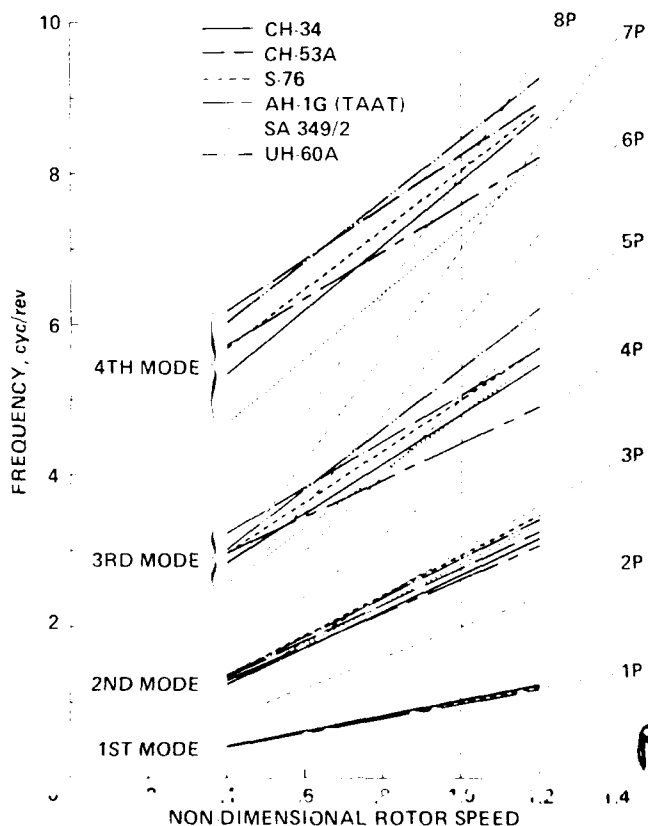


Fig. 3. Calculated flap mode frequencies.

1A-1

The flap mode frequencies are similar for all of the helicopters studied here. The second mode frequencies range from about 2.6 to 2.9/rev, and this is the dominant vibratory flap bending mode for these aircraft. Frequencies of the third and fourth modes cluster around 5 and 8/rev with a range of 1/rev seen between different rotor configurations.

The vibratory flap bending moments are shown for six of the rotors in Fig. 4. Except for the CH-34 wind tunnel data, the conditions selected represent the highest advance ratio cases in the data bases. Depending upon the rotor, the advance ratio for this comparison ranges from 0.373 for the CH-53A to 0.390 for the CH-34. The lift coefficient values range from 0.0596 for the CH-34 to 0.0776 for the UH-60A. As used here, vibratory refers to harmonics three and above. The flap bending moments are shown in the nondimensional form

$$C_{FM}/\sigma = \frac{M_F}{\rho b c \Omega^2 R^4}$$

where M_F is the flap bending moment, b is the number of blades, c is the nominal blade chord, Ω is the rotor speed, and R is the radius.

The surface plots in Fig. 4 extend from 0° to 360° in azimuth and from radial station 0 to 1. The stations with available bending-moment measurements differ among the various data sets, and this must be kept in mind when the data are examined. For instance, the most inboard station for the CH-34 wind tunnel measurements was at $0.375 R$, whereas for the UH-60A measurements were taken on the blade shank at $0.113 R$, and yoke measurements on the AH-1G were obtained at $0.023 R$. The bending moment scales in Fig. 4 have been adjusted separately for each rotor to assist in the comparison.

In general, each of these rotors shows the same behavior; the vibratory loads are dominated by the second flap bending mode. This is especially noticeable on the outer portion of the blade. However, measurements at the blade root or shank show considerable differences between the rotor configurations. The SA 349/2 shows an increasing 3/rev moment at the blade root, whereas the UH-60A shows a reduction in the load. The AH-1G measurements show considerably higher harmonic behavior on the inboard portion of the blade.

The behavior of the vibratory flap bending moments at a midspan radial station is shown as a function of advance ratio and azimuth in Fig. 5 for five of the rotors. These advance ratio-azimuth plots are analogous to the radial station-azimuth plots of Fig. 4, but advance ratio replaces radial station as the second independent variable. The advance-ratio scale goes from 0 to 0.5 for each of the rotors shown, although the extent of the advance ratio data is different for each of the experimental data sets. Note that the wind tunnel data are not used for the plots that include advance ratio as an independent variable.

Figure 5 shows that the dominant 3/rev loading at the midspan of these rotors is observed over a wide range of advance ratios. The basic character does not appear to change, even well into the transition regime. In addition, the phase of the 3/rev loading is relatively constant with increases in advance ratio.

The midspan 3/rev flap bending moments are examined in more detail in Fig. 6. For comparison, the data have been scaled as indicated in the legend. The midspan moment amplitudes are low at low advance ratios, and increase rapidly in the transition regime as advance ratio increases from 0.10 to 0.15. Except in the case of the CH-34, the loads then decrease at the higher advance ratios up to 0.20 to 0.25, after which they again start to climb and become progressively higher out to the maximum advance ratio. The 2/rev bending-moment phase shows a slight decrease with increasing speed for all of the rotors. This behavior is independent of the number of blades. The phase decrease is typically 30° to 60° for the third harmonic values shown in Fig. 6, which corresponds to about 10° to 20° in terms of rotor azimuth. This phase change is comparable with the shift in the advancing-side vortex intersection that is obtained by calculation.¹⁶ The phase angle varies by approximately 90° among the rotors shown here, which is equivalent to a 30° difference in rotor azimuth. Wake calculations suggest that the vortex loading should differ by about 20° between a two-bladed and a six-bladed rotor, but no pattern based on blade number is seen in the 3/rev phase data shown here.

CHORD BENDING-MOMENT RESPONSE

The calculated chord mode frequencies are shown in Fig. 7. The AH-1G, because of its two-bladed, semi-rigid design, has a first chord mode frequency of above 1/rev, but the other rotors have typical first mode frequencies that are below 1/rev. Considerably more variation is seen in the second chord mode frequencies than was seen in the higher blade flapping modes. The CH-34 and CH-53A rotors are not as stiff as the newer rotors are, because the trailing edge pocket-type construction of the older rotors results in the chordwise stiffness being carried only by the spar. The frequency of the second mode for these rotors is 1 or 2/rev less than for the other rotors where the airfoil trailing edge contributes to blade stiffness. For the newer designs the second chord mode frequency tends to be nearly 5/rev and this mode couples strongly with the third flap and first torsion modes.

Oscillatory chord bending moments are shown in Fig. 8 for the same high-speed conditions as for the flap bending moments that were shown in Fig. 4. Oscillatory as used here refers to all harmonics one and above. The chord bending moments have been nondimensionalized in the same fashion as the flap bending moments were, and the bending-moment scale is adjusted for each rotor separately to allow comparison. The oscillatory chord moments for this high-speed condition differ among the five rotors. However, there is some similarity in behavior between the CH-34 and SA 349/2 rotors. In both cases a large 1/rev oscillation is seen at the blade root, and it is progressively reduced for stations farther out on the blade. This suggests that the loading is related to the blade root boundary condition, that is, the blade lead-lag damper. This oscillatory root loading increases with speed, as shown in Fig. 9 for five aircraft. The CH-34, the SA 349/2, and the UH-60A all show similar behavior, the dominant effect being a rapid change in the bending moment in the third quadrant of the rotor. The data in this figure show that the effect of increased airspeed is to increase the amplitude of this

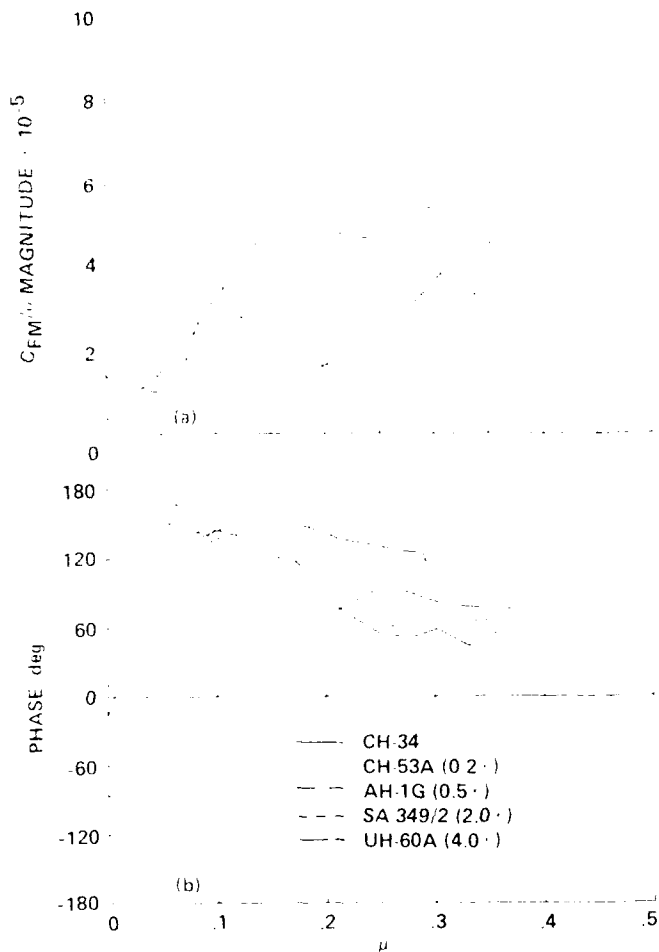


Fig. 6. Midspan 3/rev flap bending moment as a function of advance ratio for five rotors. (a) Magnitude, (b) Phase.

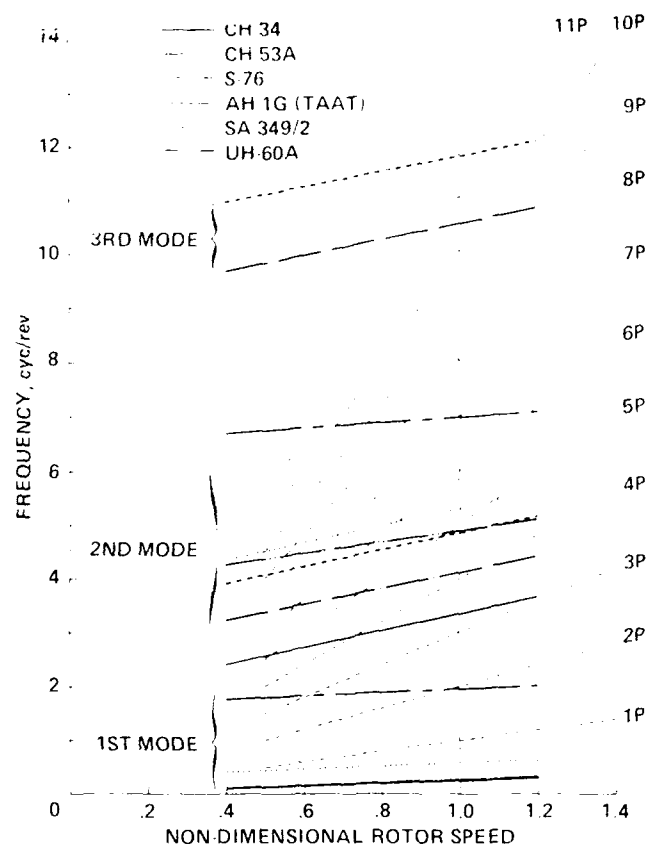


Fig. 7. Calculated chord mode frequencies.

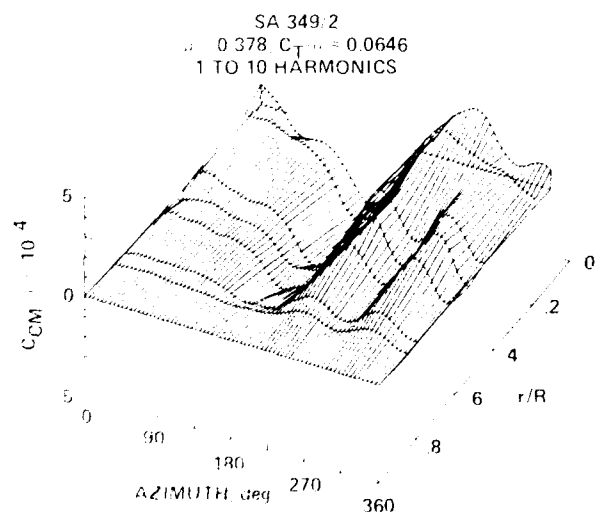
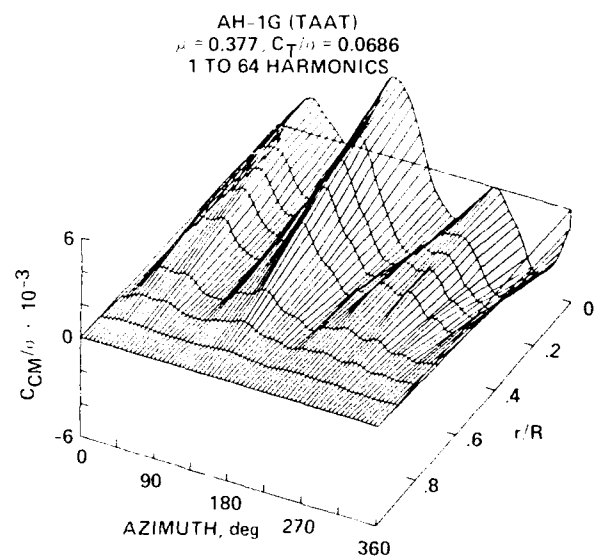
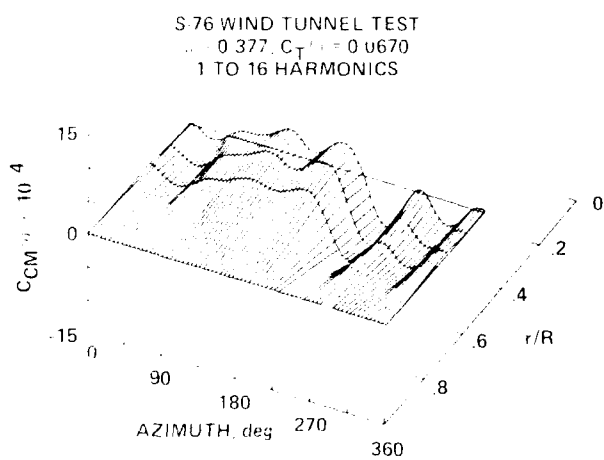
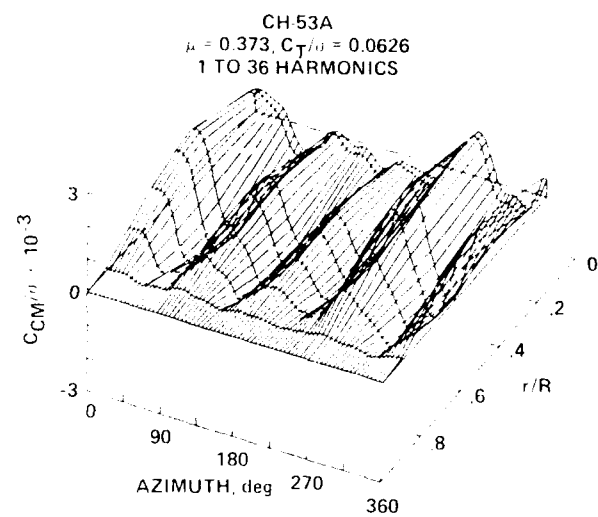
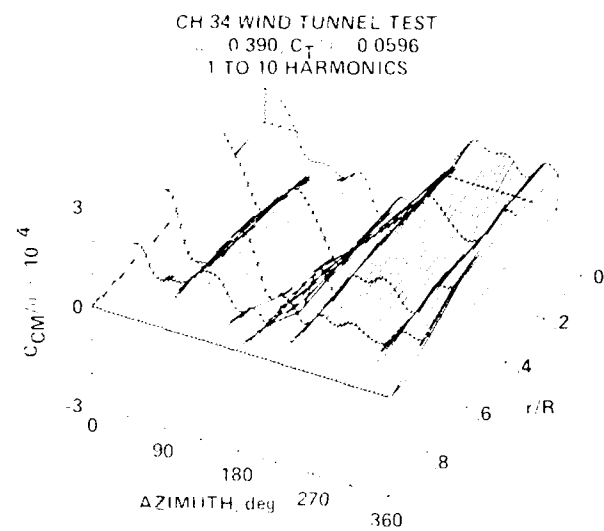


Fig. 8. Oscillatory chord bending moments for five rotors at high speed as a function of radial station and azimuth.

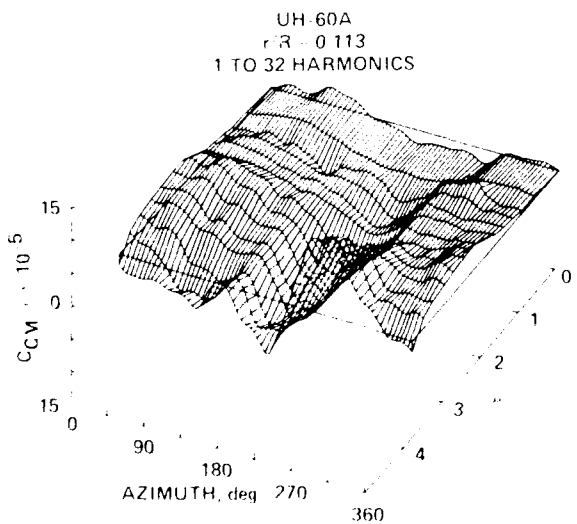
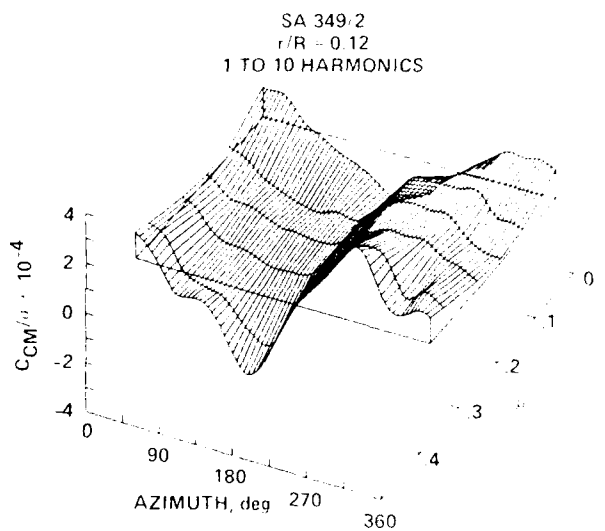
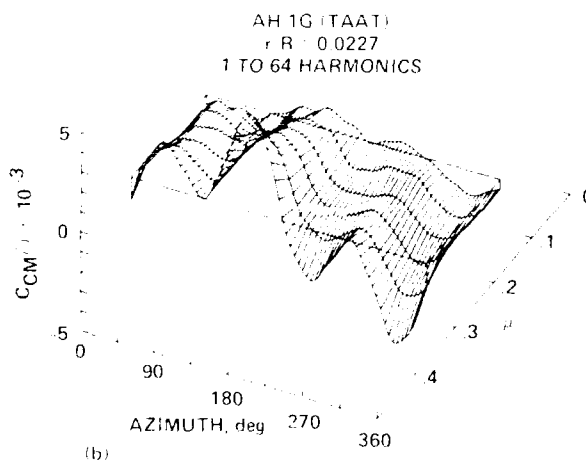
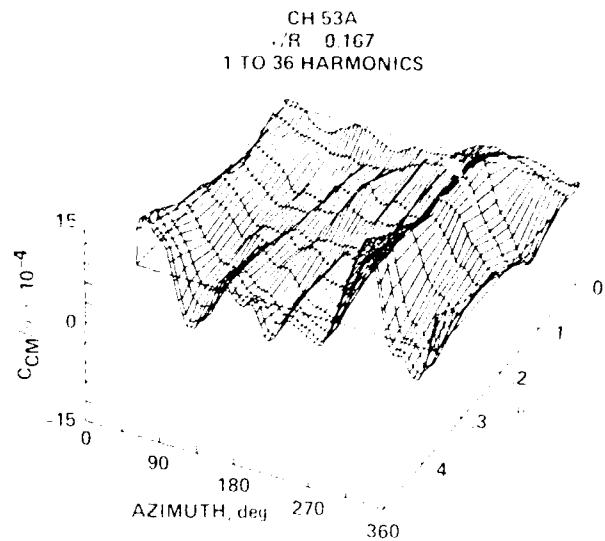
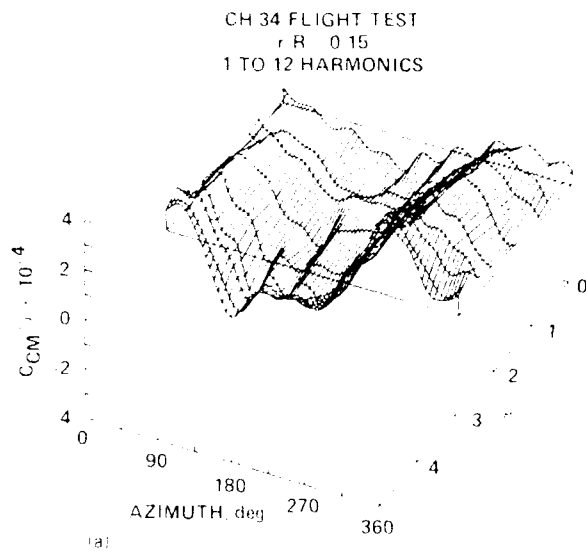


Fig. 9 Root oscillatory chord bending moments for five rotors as a function of advance ratio and azimuth.

motion. The AH-1G data also show an increase in oscillatory load with airspeed, but the azimuthal behavior is very different from that of the rotors with subcritical lag modes and their associated dampers. The CH-53A, which also uses a lead-lag damper, shows an oscillatory behavior different from that of the others.

The oscillatory root chord bending for the CH-34, the SA 349/2, and the UH-60A is further examined in Fig. 10, in which the data are scaled as indicated for comparison purposes. This figure clearly shows the rapid change in the root moment that occurs in the third quadrant. This rapid change dominates the peak-to-peak loading at this station. The CH-34 and the UH-60A use hydraulic dampers, but the damper on the SA 349/2 is elastomeric. Although differences would be expected for these two types of dampers, the loading behavior appears to be much the same. However, the CH-53A, which also uses a hydraulic damper does not show the strong 1/rev loading at the root that is seen here.

The vibratory chord bending moments for the high-speed condition are shown in Fig. 11 for five rotors. The vibratory loading of the CH-34 and CH-53A rotors is largely 3 and 4/rev; the 4/rev loading is especially noticeable on the CH-53A. The S-76 and the SA 349/2, which are stiffer in chord bending, show more response at 4 and 5/rev. Both of these rotors also show a pronounced 4/rev response at midspan on the retreating side of the disk. The vibratory loads for the AH-1G are dominated by 3/rev loading and show a continuous build-up in amplitude toward the blade root. This loading is characteristic of the first cyclic inplane mode, which has a predicted natural frequency of close to 2/rev (Fig. 7).

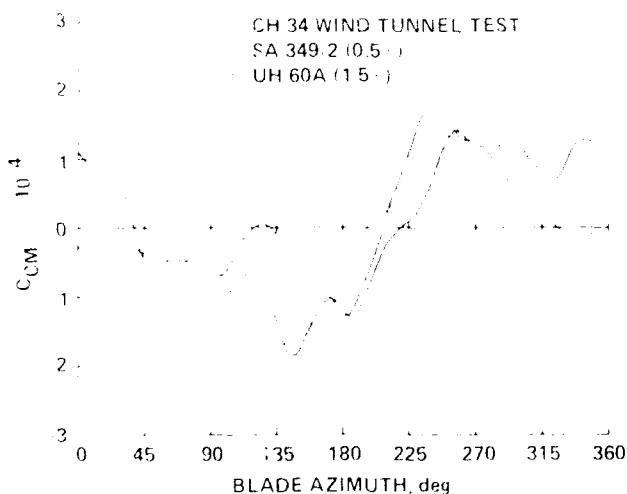


Fig. 10 Comparison of root oscillatory bending moments.
CH-34 wind tunnel test: $\mu = 0.390$, $C_T/\sigma = 0.0596$;
SA 349/2: $\mu = 0.378$, $C_T/\sigma = 0.0646$;
UH-60A: $\mu = 0.383$, $C_T/\sigma = 0.0776$.

The behavior of the vibratory chord bending moments at midspan is shown in Fig. 12 as a function of advance ratio. All of these rotors show an increase in the vibratory loading with increased airspeed. In the case of the CH-34, the CH-53A, and the AH-1G, this increase appears to be relatively smooth. The 4/rev response seen on the retreating side of the SA 349/2, however, appears to be growing quickly for advance ratios higher than 0.3.

TORSION MOMENT RESPONSE

Calculated torsion-moment frequencies are shown in Fig. 13 for six rotors. The CH-53A prediction was obtained from Ref. 17. The first torsion frequency of the AH-1G is quite low at slightly below 3/rev. The other rotors show first torsion mode frequencies that range from 4.5 to 6.0/rev. Although estimates of the uncoupled torsion mode frequencies are shown here, coupled calculations show that there can be considerable modal coupling between the first torsion, second chord, and third flap modes.

Oscillatory blade torsion moments are shown for four rotors in high-speed flight in Fig. 14. In general, there are fewer radial measurement stations for torsion than for flap or chord bending. The CH-34, the CH-53A, and the SA 349/2 data all show similar behavior in that a large, positive torsion moment is seen in the first quadrant of the rotor followed by a rapid change to a negative moment at the beginning of the second quadrant. The rotors differ in their behavior in the third and fourth quadrants. The AH-1G torsion-moment data are similar, except that the peak positive and negative moments appear to be delayed about 45° .

The behavior of the oscillatory torsion moments at the blade root as a function of advance ratio is shown in Fig. 15. This figure shows that the positive moment in the first quadrant is dependent upon airspeed, and appears to be increasing more quickly for advance ratios above 0.3. Oscillatory behavior in the third and fourth quadrants for the CH-34 and the CH-53A appears at 5 and 6/rev and is the response of the blade to the positive-negative loading on the advancing side of the disk.

The blade pitch-link load measurements are shown in Fig. 16 as a function of advance ratio and azimuth. The nondimensional pitch-link load is defined as

$$C_{PL}/\sigma = \frac{P}{\rho b \Omega^2 R^4}$$

where P is the pitch-link force. The pitch-link loads show the same behavior with advance ratio that was seen for the blade root torsion measurements in Fig. 15, as is to be expected. Pitch-link load data from the rectangular-tip blade of the research Puma and

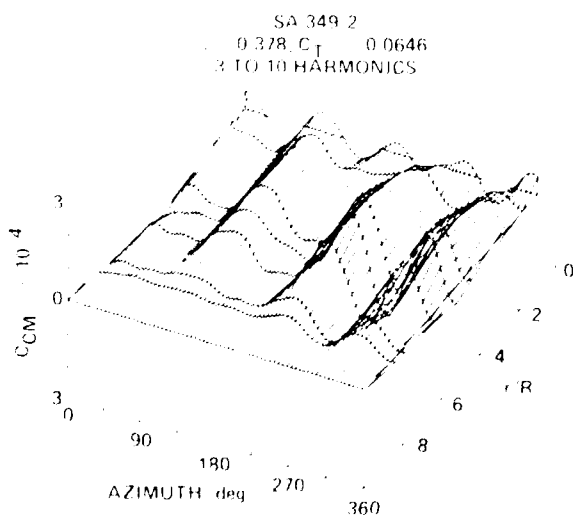
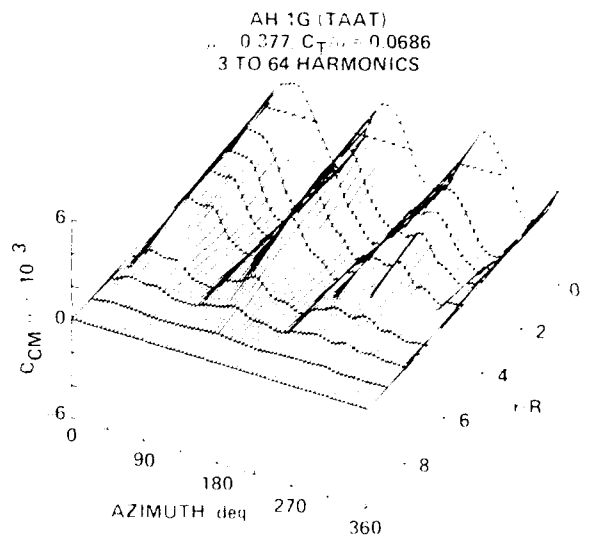
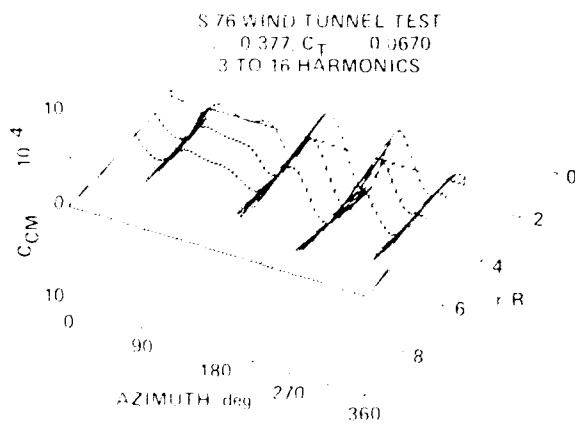
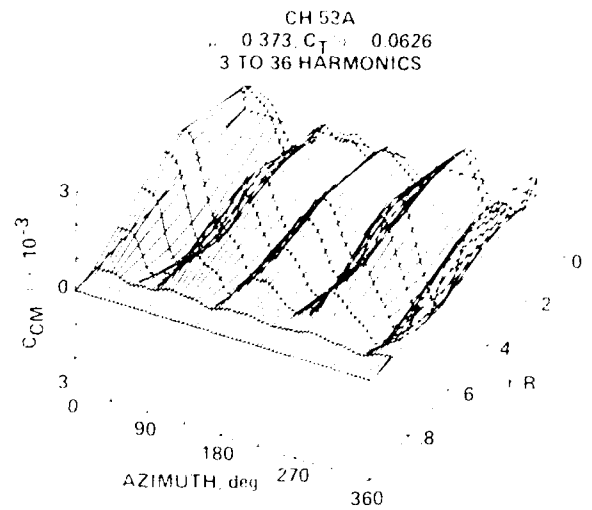
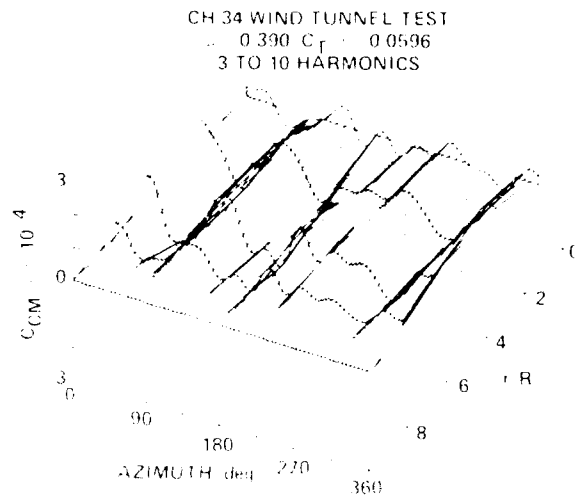


Fig. 11 Vibratory chord bending moments for five rotors at high speed as a function of radial station and azimuth.

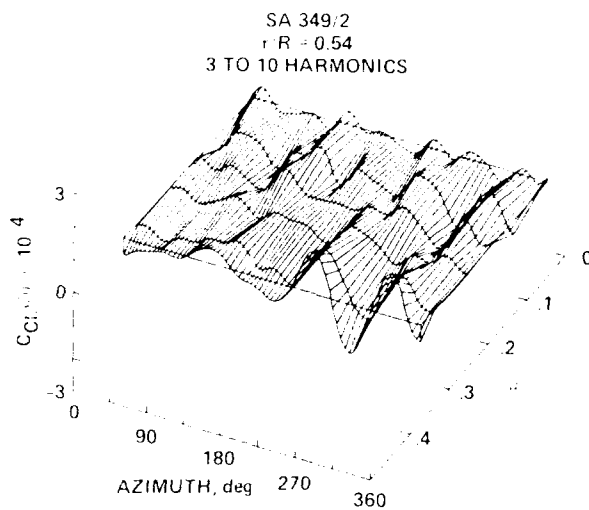
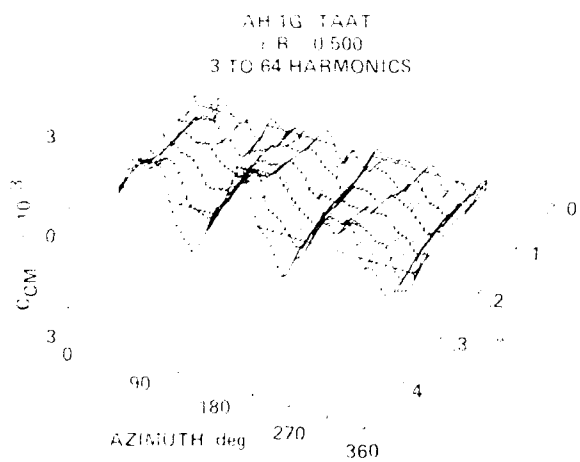
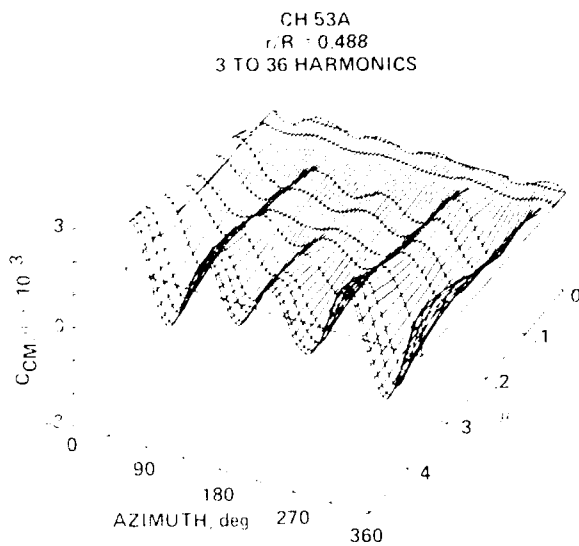
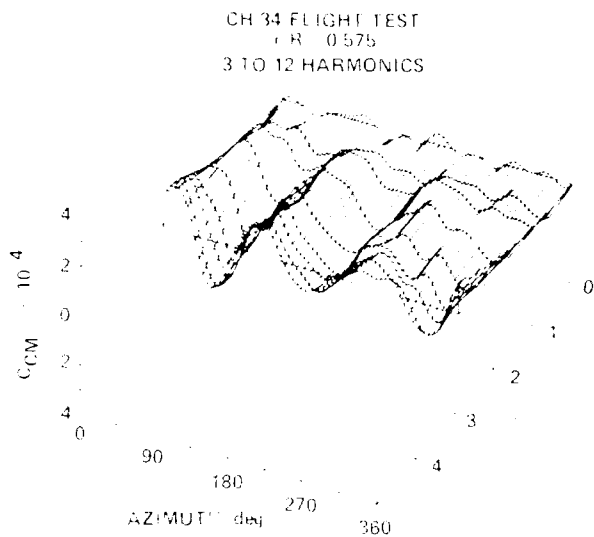


Fig. 12 Midspan vibratory chord bending moments for four rotors as a function of advance ratio and azimuth.

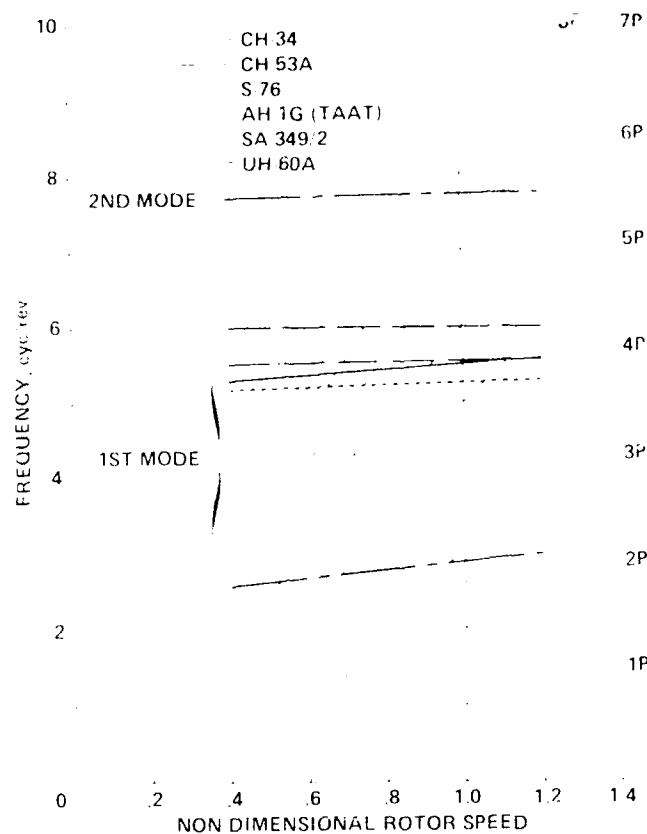


Fig. 13. Calculated torsion mode frequencies.

the UH 60A are shown here as well. As with the other rotors, a positive moment in the first quadrant switches to a negative moment at the beginning of the second quadrant. Both the Puma and the UH-60A rotors show an approximately 4/rev oscillatory response on the retreating side of the disk. The CH-34 and the CH-53A show a response at 5 and 6/rev, as was noted previously for the torsion moments. The AH-1G behavior differs from that of the other rotors in phase and in the amplitude of the pitch-link loads on the retreating side of the disk.

The pitching moment at $.95R$ on the rectangular tip of the Puma is shown in Fig. 17. A direct correspondence can be seen between the moment measurements obtained near the tip of the blade and the pitch-link loads on the advancing side of the disk. It is clear in this case that the moment at the blade tip is primarily responsible for the large change in the loading that is seen on the advancing side of the disk. On the retreating side of the disk, the pitching moment shows only a slight variation whereas the pitch-link loads are seen to oscillate at about 4/rev in response to the moment excitation.

Figure 18 shows a comparison of the azimuthal behavior of the pitch-link loads for five rotors at high speed. The pitch-link loads for all of the rotors are plotted to the same scale. The behavior of these five rotors is strikingly similar, particularly in the first quadrant. All show a positive load that peaks at roughly 45° . The moment then decreases rapidly and reaches a minimum in the second quadrant, for most of the rotors. After this minimum, the CH-53A, SA 330, and UH-60A rotors show an oscillatory response of between 4 and 6/rev which is the blade response at its first torsional mode frequency.

The oscillatory pitch-link loads increase with advance ratio, as shown in Fig. 19. The pitch-link loads of the unmodified or standard blade of the SA 330 are included here as well as the loads of the instrumented, rectangular-tip blade. The increase in the pitch-link loads is relatively uniform for the CH-53A and UH 60A rotors, but the SA 330 data show a break in the loads at an advance ratio of about 0.25, with the load amplitude increasing much faster at the higher advance ratios. The SA 349/2 behavior appears to lie somewhere in between.

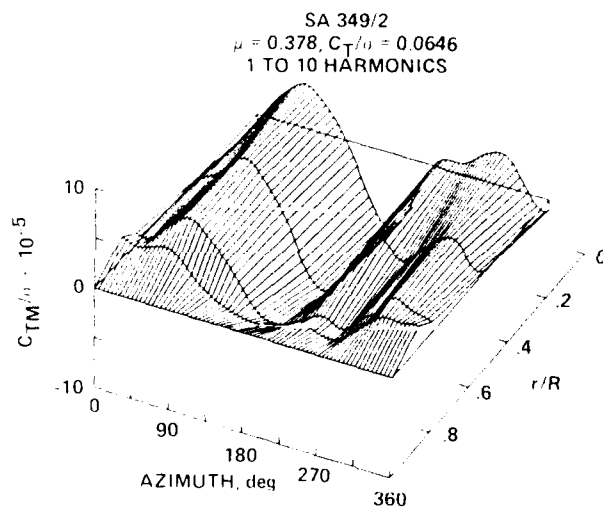
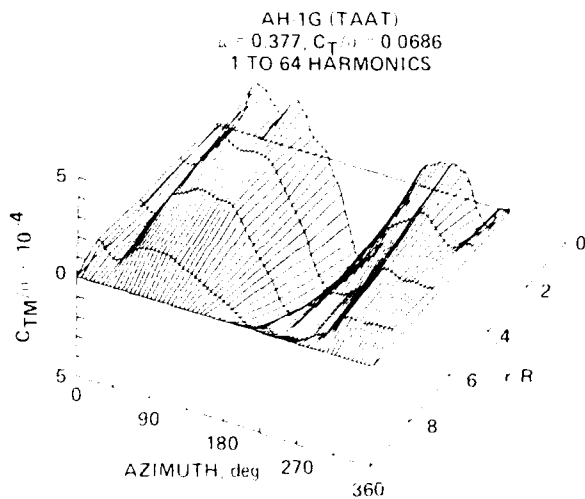
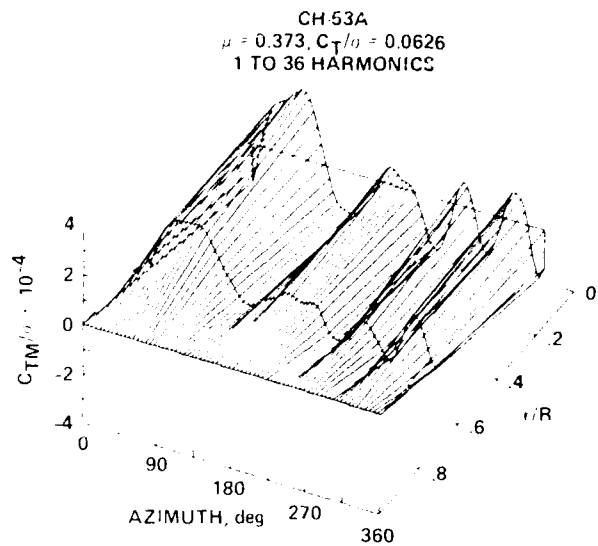
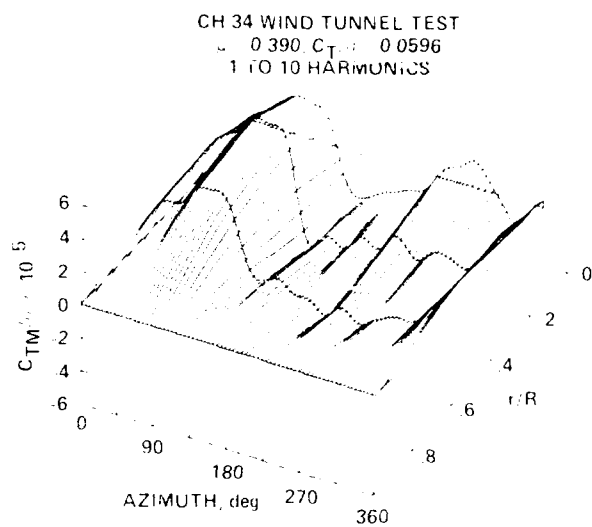


Fig. 14. Oscillatory torsion moments for four rotors at high speed as a function of radial station and azimuth.

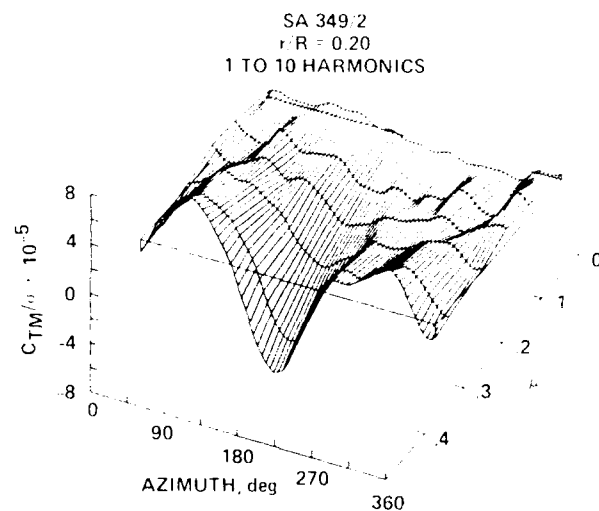
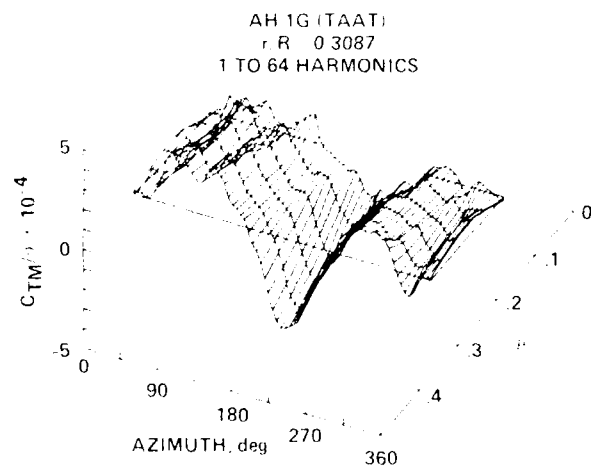
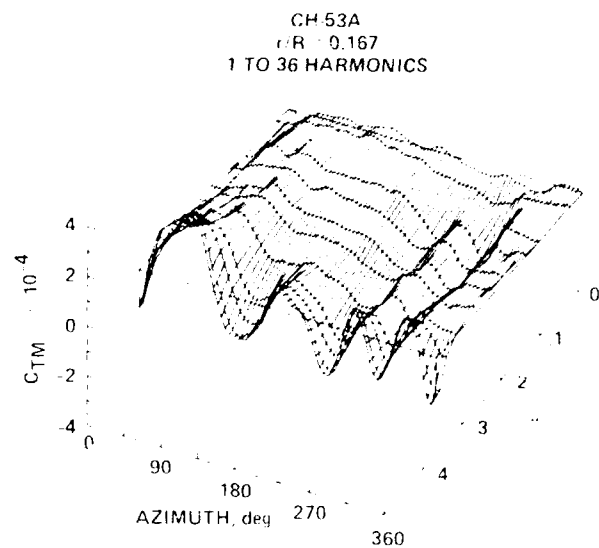
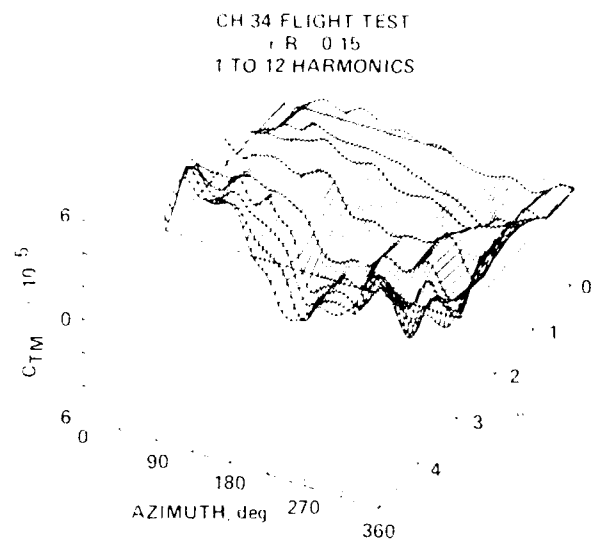


Fig. 15. Root oscillatory torsion moments for four rotors as a function of advance ratio and azimuth.

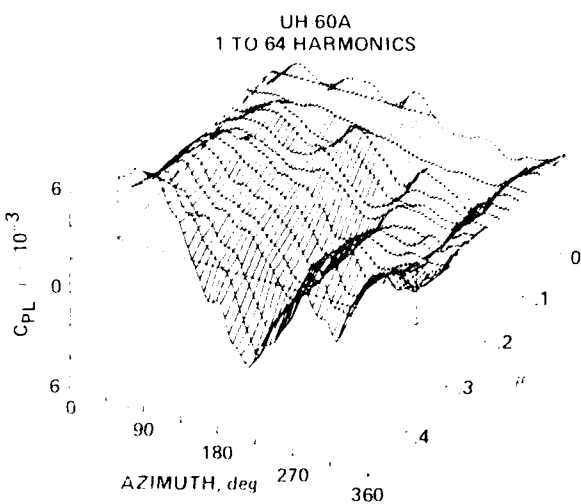
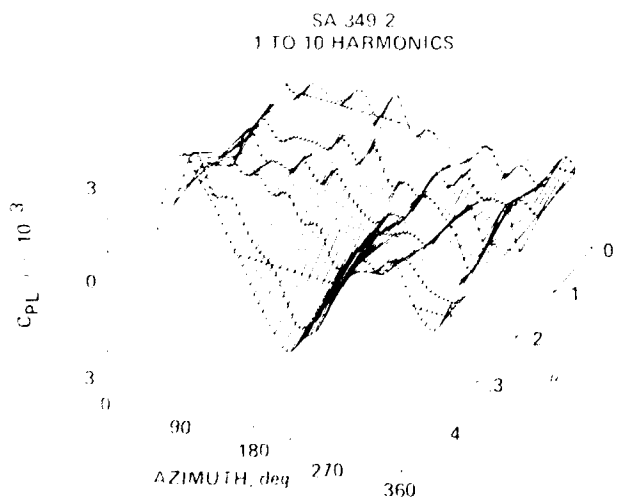
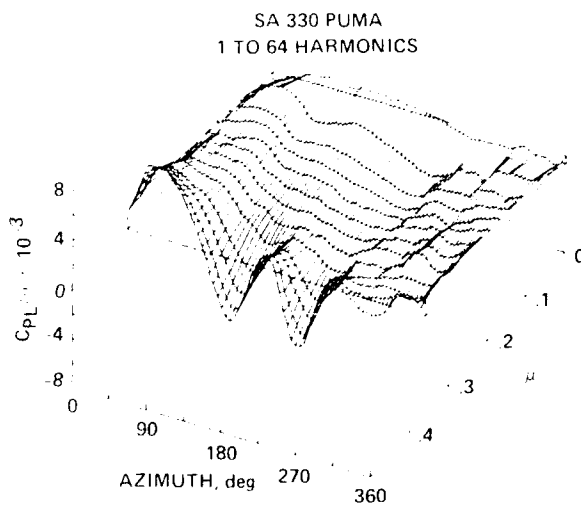
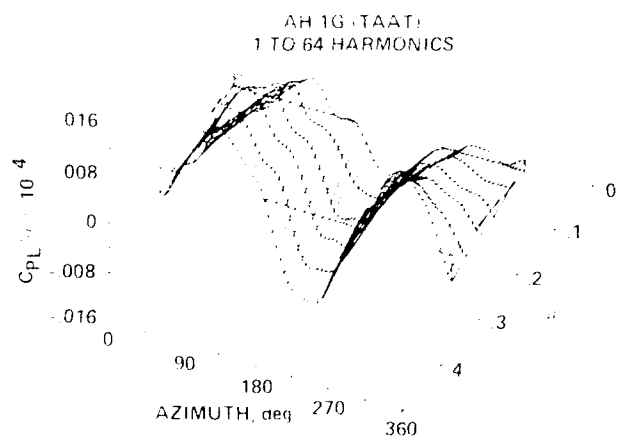
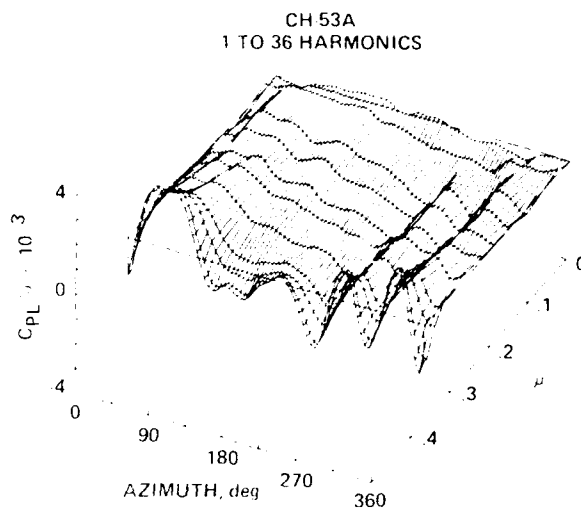
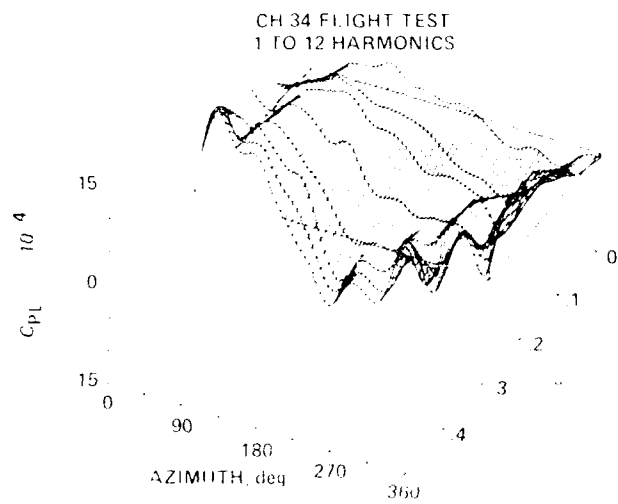


Fig. 16 Oscillatory pitch link loads for six rotors as a function of advance ratio and azimuth.

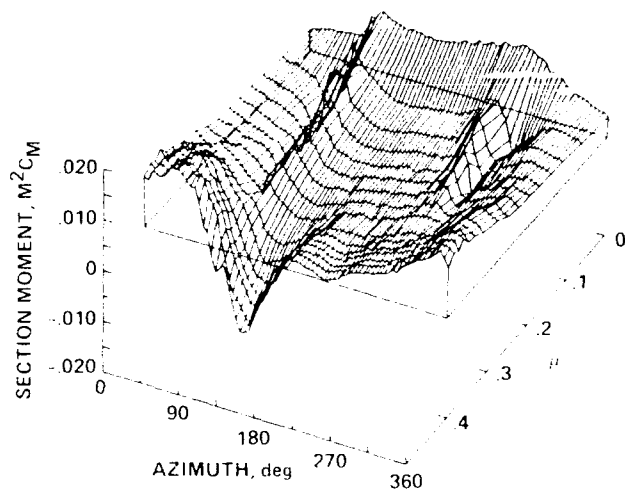


Fig. 17. Pitching moment on SA 330 rectangular-tip blade as a function of advance ratio and azimuth; $r/R = 0.95$.

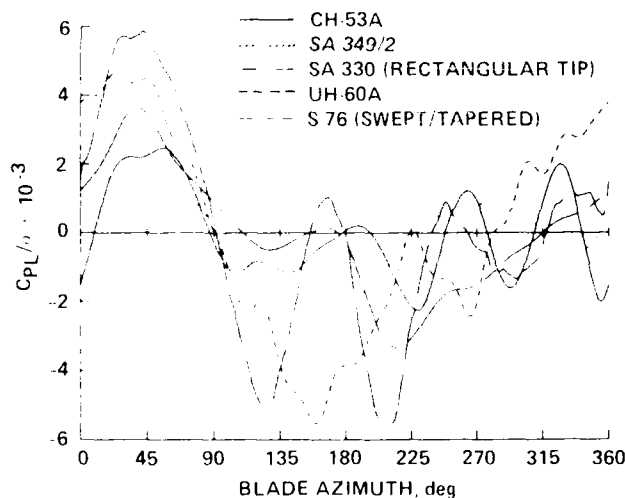


Fig. 18. Oscillatory pitch-link loads as a function of azimuth at high speed for five rotors.

CH-53A: $\mu = 0.373$, $C_T/\sigma = 0.0626$;
 SA 349/2: $\mu = 0.378$, $C_T/\sigma = 0.0646$;
 SA 330: $\mu = 0.364$, $C_T/\sigma = 0.0801$;
 UH-60A: $\mu = 0.383$, $C_T/\sigma = 0.0776$;
 S-76: $\mu = 0.377$, $C_T/\sigma = 0.0670$.

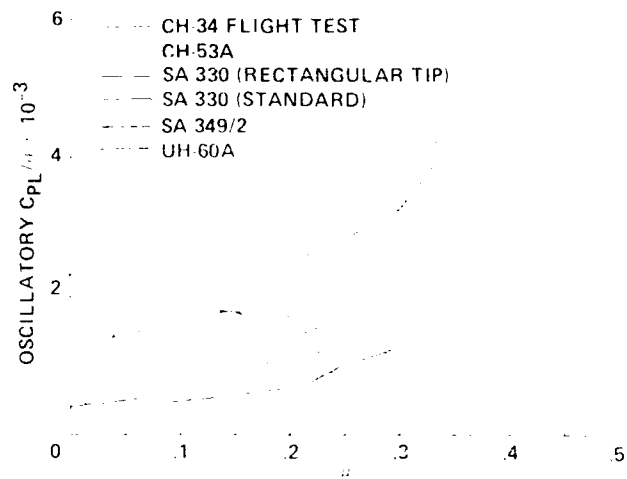


Fig. 19. Half peak-to-peak pitch-link loads as a function of advance ratio for six rotors.

The calculation of the aerodynamic pitching moment on the research Puma has been investigated recently with a number of theoretical approaches.¹⁸ In Fig. 20, the theoretical predictions of the CAMRAD/JA analysis are compared with lift and pitching-moment measurements obtained on the rectangular-tip blade. The lift coefficient is shown as a function of the local Mach number in Fig. 20(a), and the airfoil table values of lift as a function of angle of attack and Mach number that were used for the calculation are shown as an overplot. This presentation method is useful in showing that the blade is operating for the most part below the nonlinear transonic regime where unsteady transonic effects become important in the calculation of lift and moment. The CAMRAD/JA-predicted lift is similar to the measured lifts, although the small negative-lift region seen in the measurements at the highest speeds is not matched by the predictions. In the case of the pitching moment shown in Fig. 20(b), sizeable differences are seen between the predictions and measurements. The moment from the airfoil tables is shown for a 1° angle of attack and this shows that over most of the disk the steady value of the pitching moment is 0 for this symmetric profile. Thus, the major contributor to the pitching moment is the unsteady aerodynamics. Calculations based on thin-airfoil theory appear satisfactory at inboard stations where the moment is lower, but they underestimate the moment at the blade tip.¹⁸ This indicates that the three-dimensional effects at the blade tip also play an important part in the excitation of the torsional response.

The AH-1G torsion moments and pitch-link loads are quite different from those of the various articulated rotors, as noted in the discussion of Figs. 14-16. Figure 21 compares the pitch-link loads measured on the AH-1G with those measured on the UH-60A, plotted on the same scale. The torsion behavior of the AH-1G shows a strong 2/rev oscillation, and the loads are much the same on both the advancing and the retreating sides.

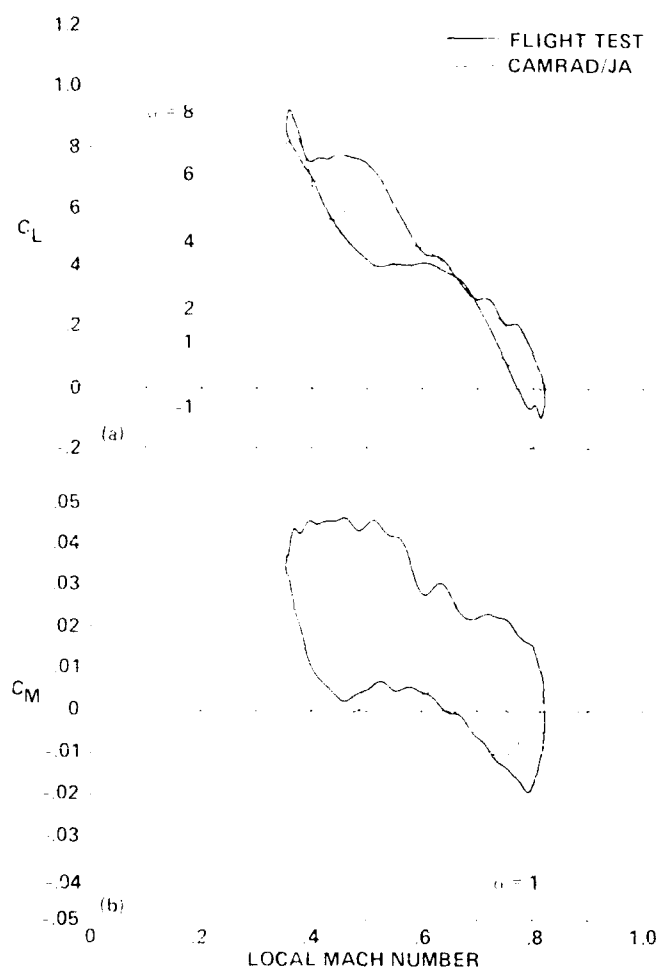


Fig. 20. Comparison of theory and experiment for lift and pitching moment as functions of local Mach number on the SA 330 rectangular tip; $r/R = 0.95$, $\mu = 0.376$, $C_T/\sigma = 0.0798$. (a) Lift coefficient, (b) Moment coefficient.

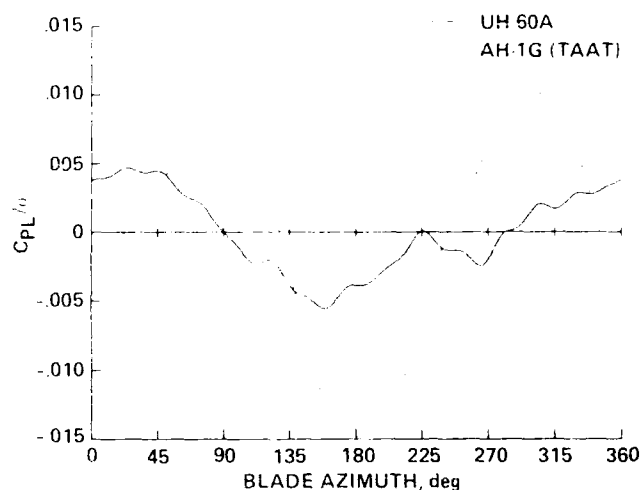


Fig. 21. Comparison of AH-1G and UH-60A pitch-link loads. AH-1G: $\mu = 0.377$, $C_T/\sigma = 0.0686$; UH-60A: $\mu = 0.383$, $C_T/\sigma = 0.0776$.

CONCLUSIONS

Data obtained in the testing of eight full-scale rotors have been compared to examine the structural response of helicopters to the oscillatory and vibratory loads in high-speed flight. Similarities and differences in the helicopter structural response are observed, and the prediction of both represent necessary tests for the development of theoretical prediction methods.

Those behaviors that are consistent between rotors and are largely independent of rotor configuration provide a first test of theoretical methods. A theoretical method that is to be used for oscillatory or vibratory load prediction must be able to predict these behaviors in a reasonably consistent manner. The major similarities observed include:

1. The dominant flapping vibratory response occurs at 3/rev. This response shows an initial peak in the transition regime, then is reduced, and then climbs again for advance ratios above 0.20 or 0.25. The phase of the 3/rev response is reduced slightly with advance ratio, and no differences in the phase response can be attributed to rotor type or blade number.
2. The root oscillatory chord bending for the CH-34, the SA 349/2, and the UH-60A show a negative to positive loading at the beginning of the third quadrant. The way in which this load builds up as the blade root is approached suggests that the loading is directly related

to the lead-lag damper. The lead-lag dampers on these rotors include both hydraulic and elastomeric designs, each with different kinds of nonlinear behavior. Despite these differences, the time history of the loading appears much the same.

3. The blade torsion moments and the pitch-link loads for the articulated rotors examined at high speed all show a large positive moment in the first quadrant that switches to a negative moment in the second quadrant. Following this positive-negative excitation, the blades appear to oscillate at the first torsion frequency, although this behavior is not the same for all of the rotors. This torsional response appears to be caused by the unsteady pitching moment at the blade tip on the advancing side of the rotor.

The differences seen in rotor response behavior that are configuration dependent provide the basis for a second test of theoretical methods to be used for the prediction of rotor oscillatory and vibratory loads. The more significant differences in the response of the rotors examined include:

1. The vibratory chord bending-moment behavior of the rotors differs significantly. In some cases, such as for the CH-53A, the response occurs mostly at the second chord mode natural frequency and, in this sense, is very similar to the flap bending-moment response. Other rotors, however, show a response at more than one harmonic, and these responses show more differences than similarities. The second chord mode is proximate to the third flapping and first torsion modes for most of the rotors examined, and the coupling of these modes may be a primary reason for the differences seen.
2. The CH-53A root oscillatory chord bending does not show the same damper-induced behavior that is seen on the CH-34 and UH-60A rotors, which also have hydraulic lead-lag dampers.
3. The AH-1G shows torsion and pitch-link load behavior that is different from that of the articulated rotors examined. The peak loading is delayed approximately 45° from that of the other rotors, and the loads are as high on the retreating side of the disk as on the advancing side.

ACKNOWLEDGEMENTS

Ruth Heffernan and Bill Warmbrodt are acknowledged for their help in obtaining SA 349/2 and S-76 data in magnetically stored form. Jeff Cross is acknowledged for his help in providing the AH-1G (TAAT) data as DATAMAP output files. Peter Wilby of the Royal Aerospace Establishment is acknowledged for allowing publication of the Puma data shown in this paper.

REFERENCES

- ¹ Hooper, W. E., "The Vibratory Airloading of Helicopter Rotors," *Vertica*, vol. 8, 1984, pp. 71-92. Also: Paper No. 46, Ninth European Rotorcraft Forum, Sep. 1983.
- ² Scheiman, James, "A Tabulation of Helicopter Rotor-Blade Differential Pressures, Stresses, and Motions as Measured in Flight," NASA TM X-952, 1964.
- ³ Rabbott, J. P., Jr.; Lizak, A. A.; and Paglino, V. M., "A Presentation of Measured and Calculated Full-Scale Rotor Blade Aerodynamic and Structural Loads," USAAVLABS TR 66-31, 1966.
- ⁴ Beno, Edward A., "CH-53A Main Rotor and Stabilizer Vibratory Airloads and Forces," SER 65593, June 1970.
- ⁵ Johnson, Wayne, "Performance and Loads Data on a Full-Scale Rotor with Four Tip Planforms," NASA TM 81229, 1980.
- ⁶ Cross, Jeffrey L. and Watts, Michael E., "Tip Aerodynamics and Acoustics Test," NASA RP 1179, Dec. 1988.
- ⁷ Heffernan, Ruth and Gaubert, Michel, "Structural and Aerodynamic Loads and Performance Measurements of an SA 349/2 Helicopter with an Advanced Geometry Rotor," NASA TM 88370, Nov. 1986.
- ⁸ Riley, M. J. and Miller, Judith V., "Pressure Distributions on a Helicopter Swept Tip from Flight Tests and from Calculations," Paper No. 9, Ninth European Rotorcraft Forum, Sep. 1983.
- ⁹ Riley, M. J., "Measurements of the Performance of a Helicopter Swept Tip Rotor in Flight," *Vertica*, vol. 13, 1989, pp. 43-50. Also: Paper No. 34, Twelfth European Rotorcraft Forum, Sep. 1986.
- ¹⁰ Yamauchi, Gloria K.; Heffernan, Ruth M.; and Gaubert, Michel, "Hub and Blade Structural Loads Measurements of an SA 349/2 Helicopter," NASA TM 101040, Dec. 1988.
- ¹¹ McHugh, Frank J., "What Are the Lift and Propulsive Force Limits at High Speed for the Conventional Rotor?," American Helicopter Society 34th Annual National Forum Proceedings, May 1978, pp. 1-12.
- ¹² Bartsch, E. A., "In-Flight Measurement and Correlation With Theory of Blade Airloads and Responses on the XH-51A Compound Helicopter Rotor, Volume I -- Measurement and Data Reduction of Airloads and Structural Loads," USAAVLABS TR 68-22A, 1968.
- ¹³ Fenaughty, Ronald and Beno, Edward, "NH-3A Vibratory Airloads and Vibratory Rotor Loads," SER 611493, Jan. 1979.
- ¹⁴ Jepson, D.; Moffitt, R.; Hilzinger, K.; and Bissell, J., "Analysis and Correlation of Test Data From an Advanced Technology Rotor System," NASA CR 3714, Aug. 1983.

- ¹⁵ Shockey, Gerald A.; Cox, Charles R.; and Williamson, Joe W., "AH-1G Helicopter Aerodynamic and Structural Loads Survey," USAAMRDL TR 76-39, Feb. 1977.
- ¹⁶ Egolf, T. Alan and Landgrebe, Anton J., "Helicopter Rotor Wake Geometry and Its Influence in Forward Flight, Volume II - Wake Geometry Charts," NASA CR 3727, Oct. 1983.
- ¹⁷ Beno, Edward A., "Analysis of Helicopter Maneuver-Loads and Rotor-Loads Flight-Test Data," NASA CR-2225, Mar. 1973.
- ¹⁸ Bousman, William G.; Young, Colin; Gilbert, Neil; Toulmay, François; Johnson, Wayne; and Riley, M. J., "Correlation of Puma Airloads -- Lifting-Line and Wake Calculation," Paper No. 21, Fifteenth European Rotorcraft Forum, Sep. 1989.